Chemistry & Biology
Article

Structure-Based Dissection of the Active Site Chemistry of Leukotriene A4 Hydrolase: Implications for M1 Aminopeptidases and Inhibitor Design

Fredrik Tholander,[1] Ayumo Muroya,[2,5] Bernard-Pierre Roques,[3] Marie-Claude Fournié-Zaluski,[4] Marjolein M.G.M. Thunnissen,[2,5] and Jesper Z. Haeggström[1,*]
[1]Department of Medical Biochemistry and Biophysics, Division of Chemistry II, Karolinska Institute, S-171 77 Stockholm, Sweden
[2]Department of Molecular Biophysics, Kemicentrum, Lund University, S-221 00 Lund, Sweden
[3]Département de Pharmacochimie Moléculaire et Structurale, 4 Avenue de l'Observatoire, UFR des Sciences Pharmaceutiques et Biologiques, 75270 Paris Cedex 06, France
[4]Pharmaleads, Paris Biopark, 11 rue Watt, 75013 Paris, France
[5]Present address: Structural Biology Business Unit, Zoegene, 227-8502, Kamoshida-cho 1000, Aoba-ku, Yokohama, Kanagawa, Japan
*Correspondence: jesper.haeggstrom@ki.se
DOI 10.1016/j.chembiol.2008.07.018

SUMMARY

M1 aminopeptidases comprise a large family of biologically important zinc enzymes. We show that peptide turnover by the M1 prototype, leukotriene A4 hydrolase/aminopeptidase, involves a shift in substrate position associated with exchange of zinc coordinating groups, while maintaining the overall coordination geometry. The transition state is stabilized by residues conserved among M1 members and in the final reaction step, Glu-296 of the canonical zinc binding HEXXH motif shuffles a proton from the hydrolytic water to the leaving group. Tripeptide substrates bind along the conserved GXMEN motif, precisely occupying the distance between Glu-271 and Arg-563, whereas the Arg specificity is governed by a narrow S1 pocket capped with Asp-375. Our data provide detailed insights to the active site chemistry of M1 aminopeptidases and will aid in the development of novel enzyme inhibitors.

INTRODUCTION

Leukotriene (LT) A_4 hydrolase (LTA4H) is an M1 aminopeptidase (AP) with high affinity for N-terminal arginines of various *tri*peptides (Örning et al., 1994). It constitutes the only eukaryotic enzyme of this family with a known crystal structure (Thunnissen et al., 2001). M1 APs define a subset of the MA(E) clan of metallopeptidases, the gluzincins. Despite the fact that APs remove only a single N-terminal residue, these enzymes exhibit a variety of important biological functions, including the processing of surface antigens, the regulation of hypertension, and involvement in tumor angiogenesis (see Table S1 available online). APs are widespread in nature and are found in organisms ranging from bacteria and plants to vertebrates.

LTA4H also catalyzes the formation of the potent chemotaxin LTB_4, a key lipid mediator of the innate immune response (Haeggström, 2004; Samuelsson, 1983). In terms of catalytic parameters, the two activities of LTA4H are very similar, with k_{cat}/K_m values of about 10^6 $M^{-1}s^{-1}$, suggesting important roles for both activities, although the precise physiological role of the AP activity remains to be determined.

LTA4H folds into an N-terminal domain, a catalytic domain, and a C-terminal domain, each with ~200 amino acids (Thunnissen et al., 2001). The interface of the domains forms a cavity, where the active site is located. At the zinc binding site the cavity narrows, forming a tunnel into the catalytic domain. The opening and the wider parts of the cavity are highly polar; the tunnel is more apolar. The cavity as a whole is mostly defined by the catalytic and C-terminal domains; only a small part of the narrow tunnel is defined by the N-terminal domain.

Both enzymatic activities of LTA4H depend on the integrity of the catalytic zinc site, HEXXH, conserved in M1 and across the entire MA(E) clans of metallopeptidases (Rawlings et al., 2004). In the M1 family, the zinc binding signature is HEXXH-$(X)_{18}$-E; the two histidines and the last glutamic acid are the zinc binding ligands. All MA metallopeptidases utilize a water nucleophile, presumably activated by the glutamic acid in HEXXH, for peptide hydrolysis. The classic MA(E) peptidase is the endopeptidase thermolysin (EC 3.4.24.27), whose catalytic domain is structurally similar to that of LTA4H, despite only 7% sequence identity. Superimposing thermolysin onto LTA4H indicate that the catalytic key residues of LTA4H occupies similar positions relative to the substrate as the corresponding residues of thermolysin (Matthews, 1988), particularly with respect to residues of the conserved HEXXH motif. In any event, an even higher degree of structural similarity can be expected among the more closely related members of M1 APs such as APA (EC3.4.11.2), APN (EC3.4.11.7), and APB (EC3.4.11.6). Mutagenetic analysis has indicated that His-295, His-299, and Glu-318 coordinate the zinc, and Glu-296 is the general base catalyst in LTA4H (Medina et al., 1991; Minami et al., 1992; Wetterholm et al., 1992).

The crystal structure of LTA4H is one of three known crystal structures of zinc APs and constitutes the only eukaryotic one. None of these structures contains a bound substrate. Furthermore, a high-quality structure of any eukaryotic MA metallopeptidase complexed with a complete substrate is lacking. In fact, the only two examples of similar complexes are structures of

Table 1. Data Collection and Refinement Statistics

Data collection				
Protein	E296Q	E296Q	Wild-type	Wild-type
Ligand	Arg-Ser-Arg	Arg-Ala-Arg	RB3040	RB3041
Diffraction limits (Å)	1.46–18.3	2.3–43.4	1.81–15.7	1.89–20
λ (Å)	1.085	1.000	1.089	0.97
R_{merge}[a] (%)	5.9 (26.1)	8.5 (38.1)	6.0 (25.5)	7.8 (26)
Completeness (%)	98.2 (88.4)	90.9 (87.0)	99.2 (95.7)	97.5 (94.9)
Mean I/σ	7.8 (2.7)	8.0 (3.2)	10.8 (2.8)	14.6 (5.8)
Unique reflections	116405	30761	61817	53141
Multiplicity	4.3 (3.8)	2.54 (2.54)	4.1 (3.9)	5.7(5.7)
Space group	$P2_12_12_1$	$P2_12_12_1$	$P2_12_12_1$	$P2_12_12_1$
Cell axes (Å)	a = 78.51, b = 87.35, c = 99.77	a = 78.49, b = 87.78, c = 99.92	A = 78.33, b = 86.94, c = 99.11	a = 78.21, b = 87.23, c = 99.23
Cell angles (°)	α = β = γ = 90	α = β = γ = 90	α = β = γ = 90	α = β = γ = 90
Refinement				
R_{factor}[b]	12.5 [12.5][d]	20.9	14.9	17.5
R_{free}[c]	16.9	27.2	18.5	22.7
Rmsd, bond distance (Å)	0.015	0.03	0.017	0.019
Rmsd, bond angle (°)	2.5	2.5	1.66	1.72
Number of H_2O	794	31	674	395

Values for the highest resolution shell are shown in parentheses.
[a] $R_{merge} = \Sigma_{(hkl)}\Sigma_i|I_i(hkl) - < I(hkl) >|/\Sigma_{(hkl)}\Sigma_i I_i(hkl)$, where $I_i(hkl)$ is the *i*th observation of reflection (*hkl*) and $< I(hkl) >$ is the weighted mean of all measurements of (*hkl*).
[b] $R_{factor} = \Sigma|F_{obs} - F_{calc)}|/\Sigma|F_{obs}|$, where F_{obs} and F_{calc} are the observed and calculated structure factor amplitudes.
[c] R_{free} is the R_{factor} calculated for the test set of reflections, omitted during refinement.
[d] R factor including all data in a final round of least-squares refinement.

the very distant prokaryotic MA endo-peptidases anthrax lethal factor and botulinum neurotoxin type A (Breidenbach and Brunger, 2004; Turk et al., 2004). Thus, structural information underlying the catalytic mechanism for APs (exo-peptidases) of the M1 family is very limited.

We used LTA4H as a model system for M1 AP and determined its structure in complex with two tight slow-binding LTA4H inhibitors, RB3040 and RB3041, and two different natural peptide substrates of LTA4H, Arg-Ser-Arg (RSR) and Arg-Ala-Arg (RAR) complexed with an inactive form of LTA4H ([E296Q]LTA4H).The backbone of the inhibitors exactly match the substrate in length and are accurate analogs of the intermediate of *tri*peptide hydrolysis with a tetrahedral phosphinic-CH_2 linkage replacing the first peptide bond. This moiety provides strong zinc chelation resembling that of the tetrahedral intermediate of peptide hydrolysis (Chen et al., 1998, 2000). Together with enzyme kinetic data and molecular modeling, these structures unravel the chemical details of peptide binding and hydrolysis by LTA4H and other members of the M1 family of APs.

RESULTS AND DISCUSSION

Zinc metallopeptidases of the M1 family and MA(E) clan are a large group of enzymes involved in an array of biological functions. In spite of their cellular abundance and roles in normal homeostasis as well as in pathology, structural information and details of their catalytic machineries are scarce. One important exception is human LTA4H for which a high-resolution crystal structure is available (Thunnissen et al., 2001). In this study, we used LTA4H as a prototype for the M1 family of APs and determined its structure in complex with *natural tri*peptide substrates and transition-state mimics to detail the chemistry for substrate recognition, binding and peptide bond hydrolysis. To allow binding of peptide substrates to the active site, we used crystals of [E296Q]LTA4H, a mutant in which the peptidase activity is drastically reduced (Andberg et al., 2000; Wetterholm et al., 1992).

X-ray Data Collection and Structure Refinement

Data processing and structure refinement statistics are given in Table 1. The final models for LTA4H•RB3040, LTA4H•RB3041, and [E296Q]LTA4H•RSR were of good quality, with well-defined electron density for all but a few terminal and surface residues. The electron densities for the ligands were clearly visible in the initial Fo-Fc difference maps of the starting models. Hence, ligands could be modeled unambiguously with full occupancies. The final atomic B-factors for the inhibitors were in the same scale as the surrounding protein atoms. The Phi- and Psi-torsion angles of the models exhibit normal variability. The [E296Q]LTA4H•RAR data were of lower resolution, but the bound ligand could be readily modeled into the initial Fo-Fc difference map.

Enzyme Kinetics and Inhibition Assays

Assessment of catalytic parameters showed that mutation of Asp-375 into an Ala, (e.g., [D375A]LTA4H) had little effect on Ala-*p*-NA (Alanine-*para*-nitroanilide) hydrolysis but nearly abolished Arg-*p*-NA (Arginine-*para*-nitroanilide) hydrolysis

Table 2. Kinetic Parameters

	Wild-type LTA4H		[D375A]LTA4H		[E296Q]LTA4H	
Substrate	K_m ± SE	k_{cat} ± SE	K_m ± SE	k_{cat} ± SE	K_m ± SE	k_{cat} ± SE
Ala-*p*-NA	1.9 ± 0.3 mM	1.7 ± 0.2 s^{-1}	3.0 ± 1.8 mM	0.5 ± 0.05 s^{-1}	1.9 ± 0.5 mM	0.001 ± 0.0006 s^{-1}
Arg-*p*-NA	1.5 ± 0.2 mM	1.9 ± 0.2 s^{-1}	[b]K_{cat}/K_m ~50 $M^{-1}s^{-1}$		2.2 ± 0.4 mM	0.002 ± 0.0005 s^{-1}
[a]Arg-Ser-Arg	1.3 ± 0.1 μM	0.56 ± 0.02 s^{-1}	[c]Inhibition	[c]Inhibition	ND	ND

ND, not determined (activity below the detection limit of the tripeptidase assay).
[a] As a comparison, data determined previously for Arg-Ser-Arg are presented (Tholander and Haeggström, 2007).
[b] Activity was low and did not obey saturation kinetics within the substrate range tested, suggesting increased K_m and reduced k_{cat}. Only a rough estimation of k_{cat}/K_m possible.
[c] The substrate was not turned over at a measurable rate and instead competitively inhibited hydrolysis of Ala-*p*-NA.

(Table 2). Furthermore, the peptidase activity of human [E296Q]LTA4H was reduced more than 1500-fold for both Arg-*p*-NA and Ala-*p*-NA.

Progress curve analysis indicated that RB3040 and RB3041 are slow-binding inhibitors of LTA4H—that is, the effect of the inhibitors increased slowly over time (Figure S1). The on rate for RB3040 was 8,100 ± 700 $s^{-1}M^{-1}$ and the off rate was (160 ± 20) · $10^{-6}s^{-1}$, yielding a K_i of 20 ± 4 nM. The estimated K_i of RB3041 was similar with corresponding values of 112,000 ± 4,000 $s^{-1}M^{-1}$ and (730 ± 100) · $10^{-6}s^{-1}$, yielding a K_i of 6.5 ± 1 nM.

Overall Binding of the RSR and RAR Peptides to [E296Q]LTA4H

The *tri*peptides are bound in an extended β-structure conformation, located antiparallel to the β strand defined by residues of the GXMEN motif, with the N-terminus anchored by the zinc moiety and Glu-271 and the C terminus by Arg-563. The zinc ion of the enzyme is chelated between the α-amino group, via a direct coordinate bond, and the oxygen of the P1 (nomenclature according to Schechter and Berger [1967]) carbonyl group of the bound peptide (Figure 1). Considering only directly coordinating ligands (the four closest), the coordination of the zinc ion is distorted tetrahedral, whereas accounting also for the more distant carbonyl oxygen of the substrate yields a distorted trigonal bipyramidal geometry. Apart from its interaction with the zinc ion, the P1 carbonyl oxygen also forms a hydrogen (H) bond to the hydroxyl group of Tyr-383. In addition, the α-amino group of the bound peptide is within H-bond distance of the carboxylate oxygens of Glu-271 and Glu-318 (Figure 1).

The P1′ amide nitrogen is 2.9Å from the carbonyl oxygen of Gly-269, and the P1′ carbonyl oxygen is 2.8Å from the amide nitrogen of Gly-268; both residues are in the conserved motif

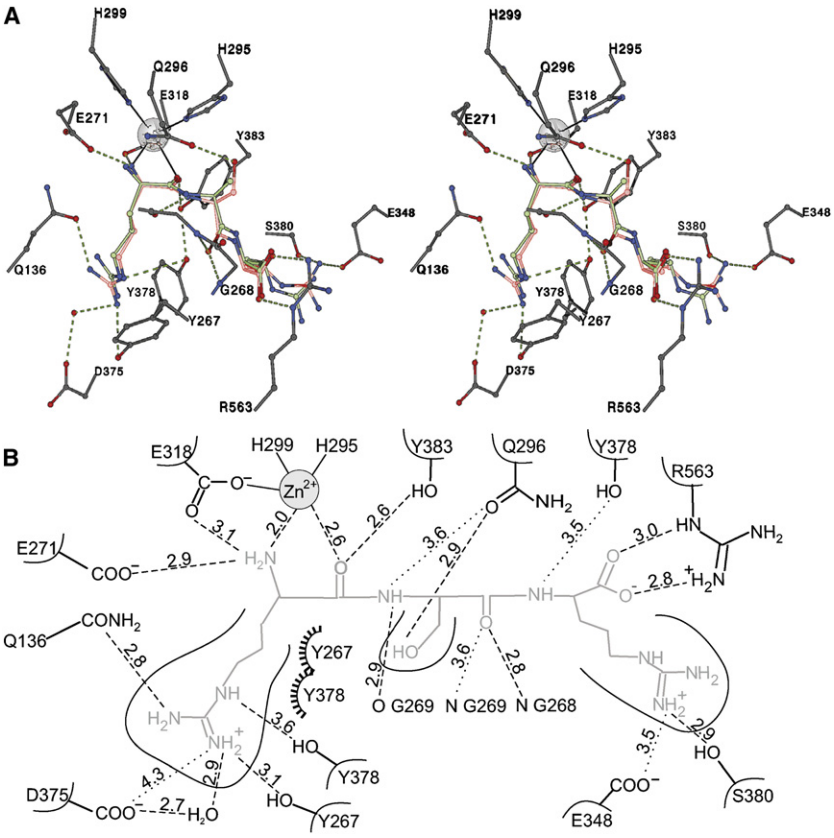

Figure 1. Binding of RSR and RAR to [E296Q]LTA4H

(A) Key binding interactions. Gray, protein carbon atoms; pink and green, RSR and RAR substrate carbon atoms, respectively. The zinc ion is shown as a reflecting sphere. Black lines, zinc coordinating bonds; green dotted lines, H bonds.

(B) Schematic representation of key interactions. Black, protein; gray, bound peptide. Nonbonding interactions are shown as dotted lines with indicated distances. Curved lines indicate subpockets.

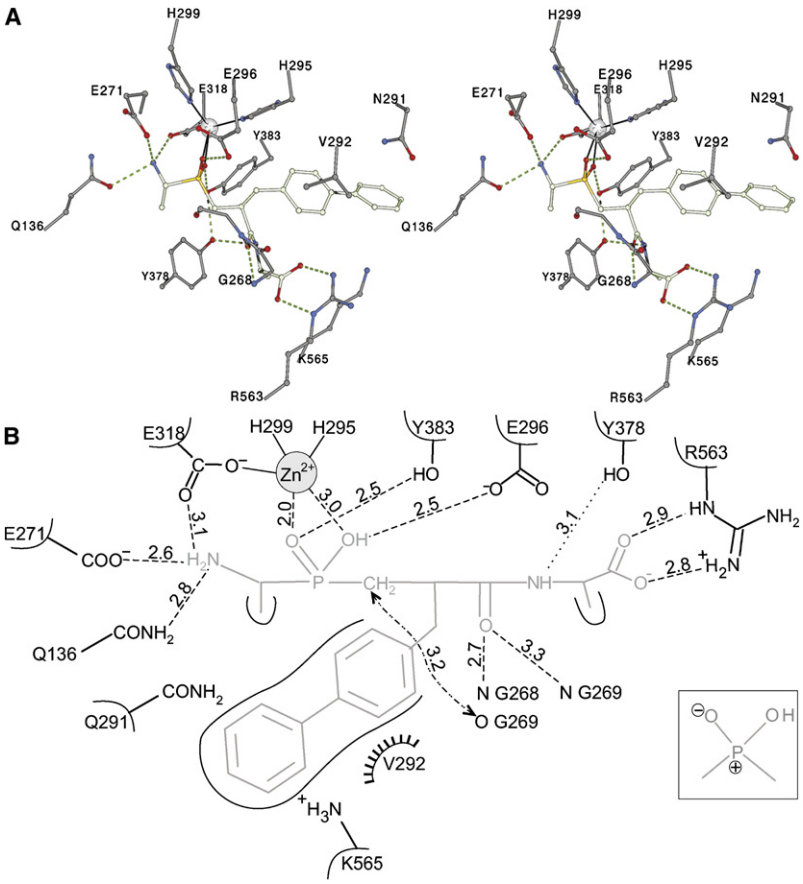

Figure 2. Binding of RB3040 to LTA4H

(A) Key binding interactions. Gray, protein carbon atoms; pale green, substrate carbon atoms. The zinc ion is shown as a reflecting sphere. Black lines, zinc coordinating bonds; green dotted lines, H bonds.

(B) Schematic representation of key interactions. Black, protein; gray, bound inhibitor. Nonbonding interactions are shown as dotted lines with indicated distances. Double arrow indicates the potential interaction for a hydrated peptide. Curved lines indicate sub pockets. Inset: Alternative description of the phosphinic moiety.

GXMEN. The P2′ amide nitrogen does not appear to form strong H bonds with the protein, since the closest group, the hydroxyl group of Tyr-378, is 3.5Å away, and at an angle incompatible with a strong H bond (N-HN-OH angle ~80°). Both oxygens of the terminal carboxylate group bind to the guanidinium group of Arg-563, a common packing arrangement.

The P1′ arginine side chain packs between Tyr-378 and Tyr-267, with H-bond distances between nitrogens of the guanidinium group and the hydroxyl group of Tyr-267 and the side chain carbonyl oxygen of Gln-136. Because the guanidinium group is close to the aromatic pi-clouds of Tyr-267 and Tyr-378, aromatic stacking and H bonding provide additional binding energy. Asp-375 is the closest residue (4.5Å away) that can provide ion pairing with the arginine side chain and contributes by H bonding mediated by a bridging water molecule.

The P1′ serine side chain of RSR forms a clear H bond with the Oε1 atom of Gln-296. Despite the lack of this H-bond RAR binds in a very similar manner. For the P2′ arginine side chain, the hydroxyl group of Ser-380 is the H-bonding partner for the guanidinium group. As with the P1 residue, a distant charged residue, Glu-348 at 3.6Å, is the closest countercharged residue. Because the P2′ arginine is not closely packed with the enzyme, no additional clear interactions occur.

When bound to LTA4H, both *tri*peptides have very similar conformations (Figure S2). Thus, a different P1′ residue does not significantly alter substrate binding; in particular, zinc coordination geometry is maintained. Despite the additional H bond between the serine hydroxyl and the Gln-296 side chain, the conformation at the zinc site is identical for both peptides. This H bond slightly changes the position of the side chain of Gln-296. The presence of a hydroxyl group leads to slightly lower K_m and k_{cat} for hydrolysis of RSR than for RAR (Tholander and Haeggström, 2007). Presumably, the additional H bond between RSR and Glu-296 increases substrate affinity (assuming that K_m to some extent reflects substrate affinity), but it also slightly disturbs the catalytic actions of Glu-296, leading to a reduced k_{cat}.

Crystal Structure of LTA4H•RB3040 and LTA4H•RB3041

Both RB3041 and RB3040 have overall binding patterns that are very similar to those of the tripeptides (Figures 1–3, Figure S2). The inhibitors bind in an extended β-structure conformation (Figures 2 and 3). Both inhibitors are firmly anchored to Glu-271

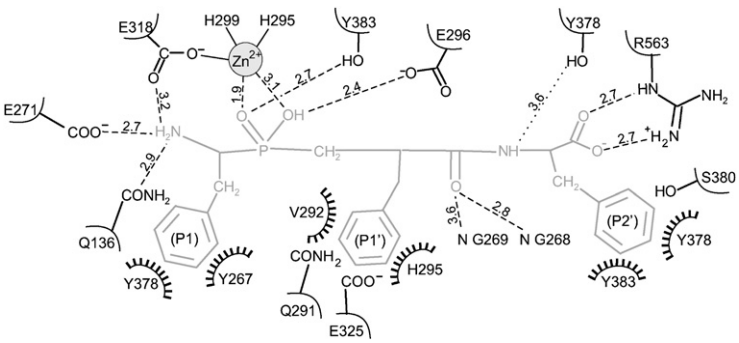

Figure 3. Binding of RB3041 to LTA4H

Nonbonding interactions are shown as dotted lines with indicated distances. Black, protein; gray, bound inhibitor.

through their N-termini and to Arg-563 through their C-termini, where two H bonds bind the carboxylate moiety to the guanidinium group. In addition to the H bond to Glu-271, the N-terminal amino group forms H bonds to Gln-136 and Gln-318. The carbonyl oxygen of the peptide bond of the inhibitor binds to the backbone nitrogen of Gly-268, and the peptide bond nitrogen binds to the hydroxyl group of Tyr-378. The phosphinic group chelates the zinc ion in a distorted bidentate fashion, with binding distances of approximately 2.0 and 3.0Å between the chelating oxygens and the zinc ion (Figures 2 and 3). Considering only the shorter interactions the total coordination geometry of the zinc becomes distorted tetrahedral, whereas if all interactions are accounted for it becomes distorted trigonal bipyramidal, as observed for the *tri*peptide ligands. Besides interacting with the zinc ion, one chelating oxygen of the phosphinic group H binds to Glu-296 (binding distance, 2.50Å) and to Glu-271 (3.28Å); the other binds to Tyr-383 (2.54Å).

Of the two inhibitors, RB3041 has more contact with the S1′-S2′ subpockets of the enzyme, because this inhibitor has three aromatic side chain substituents, whereas RB3040 has two methyl and only one aromatic (Figures 2 and 3). The P1 phenylalanine side chain of RB3041 is tightly packed with the enzyme and interacts with Gln-136, Tyr-267, Tyr-378, and Phe-314. The P1′ and P2′ phenylalanine residues are located in more spacious, water-filled cavities and do not interact extensively with the enzyme. The P1′ phenylalanine stacks with His-295 and interacts to a lesser extent with Glu-325, Asn-291, and Val-292. The P2′ phenylalanine mainly packs between Tyr-378, Tyr-383, and Ser-380.

Just as for the *tri*peptides, the main binding strength of the inhibitors is achieved through backbone interactions. The inhibition studies support this conclusion, because different side-chain substituents do not affect binding potency to any significant extent. Similar to the difference in P1′ residues of the *tri*peptides (see above), the absent P1-P1′ backbone amide nitrogen of RB3040 and RB3041 is not likely to induce a shift in binding, particularly with respect to the zinc ion, that would lead to a binding conformation more similar to the *tri*peptides. This was also supported by modeling of a tetrahedral reaction intermediate, as seen in the following section (Figure S3). In the model, the nitrogen moiety of the scissile bond was only capable of donating a single H-bond, which should not be able to disrupt the other main interactions of the backbone to any large extent.

The zinc coordination observed for the tetrahedral phosphinic group of the inhibitors reflects the binding geometry of a tetrahedral reaction intermediate. Notably, because the backbones of the inhibitor match the length of a *tri*peptide, they can be considered to mimic the main transition state of *tri*peptide hydrolysis particularly well. Except for the HOOP-CH_2 link replacing the P1-P1′ amide, they define Phe-Phe-Phe and Ala-*bi*Phe-Ala *tri*peptides. In addition to direct metal coordination, one of the chelating oxygens of the phosphinic group also interacts with the carboxylate group of Glu-296, while the other interacts with the hydroxyl group of Tyr-383. The interaction between Glu-296 and the inhibitor suggests a general base reaction mechanism; a similar interaction probably occurs between Glu-296 and an attacking water molecul, prior and during formation of the tetrahedral reaction intermediate.

Modeling of the Tetrahedral Reaction Intermediate

The modeled binding conformation of the hydrated peptide reveals that the scissile amide nitrogen and the corresponding CH_2 moiety of the inhibitor have inverted geometries with respect to each other, thus differing slightly in position (Figure 2, Figure S3). Compared with the CH_2 moiety of the inhibitor, the amide nitrogen of the modeled hydrated peptide takes a conformation that is much closer to a carboxyl oxygen of Glu-296. Actually, the NH group next to the scissile bond of the intermediate species adopts an sp^3 geometry. Thus, the lone-pair of this NH moiety faces the acidic proton of Glu-296. The proton of this group is directed toward the backbone oxygen of Gly-269. Furthermore, in the optimized binding conformation of the hydrated RAA peptide, the guanidinium of the P1 arginine forms a direct H bond with Asp-375, consistent with [D375A]LTA4H's inability to hydrolyze arginyl-*tri*peptides and Arg-*p*-NA, as seen above and in Tholander and Haeggström (2007).

The binding geometries of the modeled reaction intermediates were evaluated with a QM/MM approach with the QSite software (version 4.0; Schrödiger, New York, NY). These calculations confirmed the results of the force field-based approach and indicated that plausible binding geometries were obtained. Thus, the overall geometries of the reaction intermediates were maintained after optimization with the QM/MM approach. In addition, coordinate bonds between the oxygen atoms of the *gem*-diolate of the reaction intermediate and the zinc ion were refined to better reflect experimental data available for such interactions (Alberts et al., 1998).

Substrate Binds Along the Conserved Sequence GXMEN

In the crystal structures, interactions between the enzyme and the backbones of the inhibitors, as well as the substrates, were similar in corresponding regions. Thus, for all ligands, the peptide backbone binds as an extended β strand antiparallel to the β strand defined by the GXMEN motif, which is conserved among M1 APs.

Specificity for Peptide Chain Length Is Dictated by the Distance between Arg-563 and Glu-271

The clear interactions between the terminal groups of the different ligands with Arg-563 and Glu-271 of the enzyme show how the enzyme controls the preference for *tri*peptides (Figures 1–3). The C-termini of the two substrates and the inhibitors each form two H bonds with the guanidinium group of Arg-563. The α-amino groups of the tripeptides bind to Glu-271, Glu-318 (with a less favorable H-bonding geometry), and the zinc ion. This trivalent interaction tethers the ligand firmly to the protein.

Nature of the S1 Specificity Pocket

Various *tri*peptides are good substrates for LTA4H, and the most important determinant of efficient *tri*peptide hydrolysis is an N-terminal arginine (Örning et al., 1994). This arginyl specificity is explained by the characteristics of the S1 pocket. The pocket is deep and narrow and, in the vicinity of the Cβ-Cδ carbons of the P1 arginine side chain, lined with aromatic and hydrophobic residues. Deeper in the pocket, close to where the guanidinium group binds, a patch of polar groups exist, including Asp-375. The guanidinium group of the bound substrate is H-bonded to Asp-375 via a bridging water molecule. The electrostatic nature

of the S1 pocket indicates that the bottom of the pocket is electronegative, whereas the upper parts are more neutral, allowing long hydrophobic groups terminated with positive groups to bind (Figure S4). Thus, residues with shorter hydrophobic side chains can also bind efficiently in this pocket, as exemplified by RB3041.

Elements of the S1 Specificity Pocket Are Also Important for Catalysis

Asp-375 is essential for hydrolysis of arginyl-*tri*peptides (Tholander and Haeggström, 2007). Mutation of this residue to Ala virtually abolished hydrolysis of Arg-*p*-NA but had little effect on hydrolysis of Ala-*p*-NA (Table 2). If the P1 Arg side chain is modeled with its Cα at a position equivalent to the P1 Cα of RB3040 or RB3041, Asp-375 could form a salt bridge with the guanidinium group of the bound substrate (Figure S3). Thus, in the reaction intermediate the guanidinium group of the P1 Arg takes a position significantly closer to Asp-375 compared with the binding conformation of the *tri*peptides in the initial Michaelis complex. This would provide further binding energy to the reaction intermediate and possibly place additional strain on the scissile bond, which could facilitate its cleavage. According to the scheme outlined here, the distance between the guanidinium group of the P1 Arg and the carboxylate of Asp-375 would be gradually reduced along the reaction path. Enzyme kinetic data for [D375A]LTA4H support this notion, as seen above and in Rudberg et al. (2002b) and Tholander and Haeggström (2007).

Therefore, Asp-375 seems to be more critical for the binding of the intermediate species than the substrate, or at least to successively increase the binding strength for this interaction as the substrate moves along the reaction path. Because Asp-375 is conserved in closely related M1 APs, this residue is likely responsible for the specificity of aminopeptidase B, *Caenorhabditis elegans* AP-1, and other mammalian LTA4Hs for arginyl-peptides.

In contrast, Glu-271 could easily adapt to form strong H bonds with the α-amino group of both substrate and intermediate. However, mutational data suggest that this interaction is more crucial for binding of the transition state, as exemplified by more pronounced effects on k_{cat} than on K_m upon mutation of this residue in LTA4H and APN (Luciani et al., 1998; Rudberg et al., 2002a). Therefore, it is possible that also this interaction becomes optimized as the reaction proceeds.

Nature of the S1′ and S2′ Specificity Pockets

The *bi*-phenyl and phenyl moiety of RB3040 and RB3041, respectively, probe the S1′ pocket, which is formed at the interface between the catalytic and C-terminal domains of LTA4H. The pocket is large, water-filled, and lined with polar residues (Asn-291, Glu-325, Arg-326, Glu-533, and Lys-565), allowing both bulky and polar residues to be accommodated in the P1′ position.

Örning et al. (1994) proposed a preference for hydrophobic residues at the S1′ position. Such groups definitely fit into this large cavity, as exemplified by the P1′ *bi*-phenyl residues of RB3040, but they do not pack favorably with the enzyme and add little binding energy. Instead, polar side chains of variable size could easily form specific interactions.

The very similar S2′ pocket is also formed at an interface between the catalytic and C-terminal domains. It may be viewed as a large intrusion of the protein surface and the entrance to the active site. Side chains of bound P2′ residues face the outside of the protein. The S2′ pocket is large and the bound P2′ arginines of the *tri*peptides have few contacts with the protein. The only specific interactions are H bonds between the bound guanidinium group and Ser-380 and a possible electrostatic interaction with Glu-348. Similarly, the P2′ phenyl moiety of RB3041 binds at the same location and does not exhibit distinct interactions.

Substrate Binding in the Michaelis Complex Is Compatible with Polarization of the Scissile Carbonyl Bond

When a *tri*peptide binds to the enzyme, the carbonyl oxygen of the scissile bond interacts with the zinc ion and the hydroxyl group of Tyr-383 while the amide nitrogen interacts with the backbone carbonyl of Gly-269 (in the GXMEN motif). This positions the scissile peptide bond optimally for catalysis, presenting the carbonyl carbon to both Glu-296 and the nucleophilic water. Together, Tyr-383 and the zinc ion polarize the carbonyl bond of the scissile peptide bond (Figures 4A–4B). This increases the electropositivity of the carbonyl carbon, facilitating the nucleophilic attack of a water molecule.

The Intermediate Oxyanion Is Stabilized by Tyr-383 and the Zinc Ion

The interaction between Tyr-383 and the inhibitor corresponds to an interaction between the oxyanion of the reaction intermediate and the enzyme. Thus, Tyr-383 and the zinc ion define an oxyanion stabilization site, similar to the oxyanion hole of serine proteases (Figure 4B) (Robertus et al., 1972). The similarity between the tetrahedral reaction intermediate (a *gem*-diolate) and the inhibitors becomes even more evident if one considers the fact that the phosphinic moiety of the inhibitors could be described by a charge-separated species with a positively charged phosphor atom and a negatively charged phosphonyl oxygen, and not only with neutral atoms (Figure 2, inset).

In the distantly related thermolysin (7% sequence identity but significant structural similarity), the corresponding residue of Tyr-383 is His-231, which is believed to participate in peptide hydrolysis in two ways (Beaumont et al., 1995; Mock and Aksamawati, 1994; Mock and Stanford, 1996). It can serve as a general base catalyst or, as we propose for Tyr-383 in LTA4H, it can stabilize the intermediate oxyanion of the hydrated peptide. The latter mechanism is currently the most widely accepted, partly because the former leaves the role of the conserved Glu of the HEXXH motif undefined and was based on analysis with inefficiently hydrolyzed substrates (Barret et al., 1998). In other MA metallopeptidases, corresponding residues may well fulfill the same task. For example, the tricorn-interacting factor F3 (an M1 AP), the anthrax lethal factor (an M34 endopeptidase) and tentoxilysin (an M27 endopeptidase) all have Tyr residues at positions suggesting similar roles. In carboxypeptidase A, an M14 carboxypeptidase of the MC clan, a corresponding arginine serves this purpose (Phillips et al., 1990).

Plausible Positioning of the Hydrolytic Water Is Compatible with Weak Zinc Coordination

The complexes between [E296Q]LTA4H and the peptides lack electron densities interpretable as a possible hydrolytic water

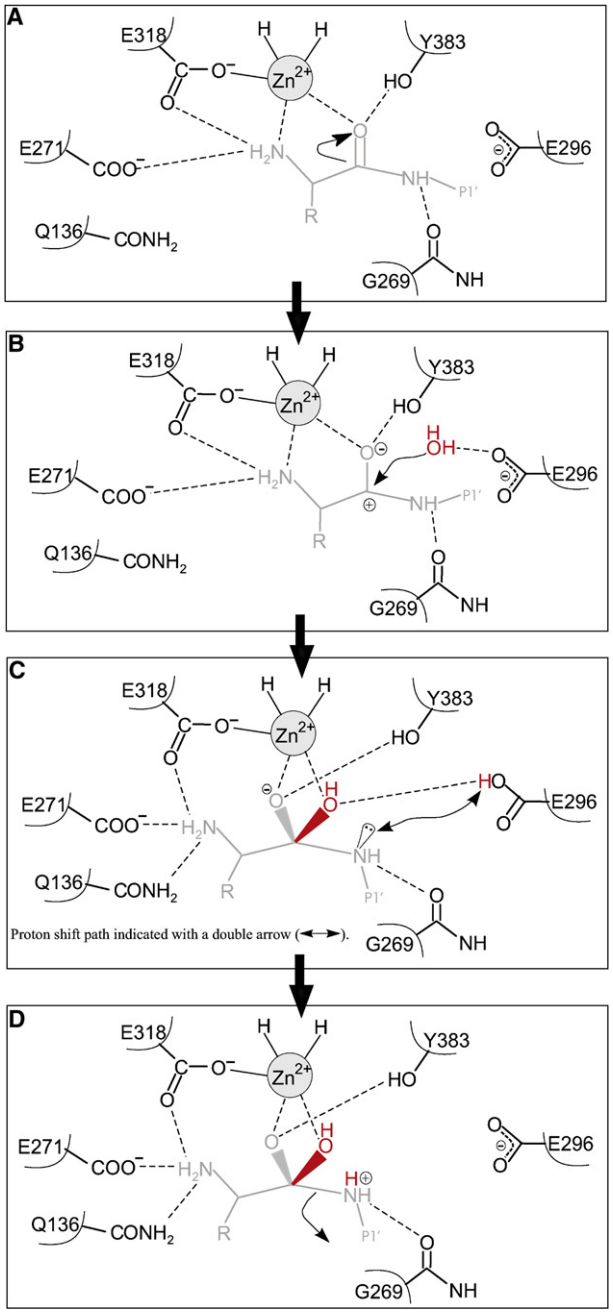

Figure 4. Reaction mechanism for peptide hydrolysis by LTA4H

(A) Substrate displaces the zinc-associated water molecule and chelates the zinc ion by its free amine and carbonyl oxygen, the former with a direct coordinate bond. The carbonyl oxygen also forms a strong H-bond with the hydroxyl group of Tyr-383. The binding arrangement polarizes the carbonyl bond and increases the electropositive character of the carbonyl carbon.

(B) The polarized carbonyl carbon is susceptible to nucleophilic attack. To further assist in the nucleophilic attack by water (in red) Glu-296 acts as a base.

(C) Upon formation of the tetrahedral reaction intermediate the substrate becomes slightly shifted, leading to exchange of zinc-coordinating groups and strengthened H bonds to nearby residues. The amino moiety H bonds tighter to Glu-271 and the oxyanion forms two strong bonds, a coordinate bond to the zinc ion and a low-barrier hydrogen bond to Tyr-383. The oxygens of the hydrated carbon form the same type of zinc coordination geometry as the free amine and carbonyl oxygen of the substrate, a distorted trigonal bipyramidal coordination geometry is maintained with one directly coordinating group and one group at a slightly longer distance. As a result of previous base catalysis, an acidic proton resides on a carboxylate oxygen of Glu-296. This proton is directly shuffled to the leaving amine moiety, which in this binding conformation has adopted a tetrahedral geometry, allowing it to present its lone pair to the protonated Glu-296, thus facilitating the proton transfer. (Note that the conformational change does not take place in the P1′ residue, as suggested by the figure, but is localized to the zinc-coordinating groups.)

(D) Once protonated, the amine constitutes a good leaving group. The positional shift associated with formation of the reaction intermediate could be partly driven by a force exerted by Glu-271 and Asp-375 (left out of the diagram for clarity, but further discussed in the text), which may also facilitate the final breakdown of the substrate.

molecule. Presumably, the bound peptide has displaced the water molecule, and the absence of a charged Glu-296 prevents a new water molecule from binding when substrate is present. Notably, bound inhibitors commonly displace hydrolytic waters from the coordination sphere of a catalytic zinc (Alberts et al., 1998). However, in LTA4H•RB3040 and LTA4H•RB3041, one of the oxygen atoms of the phosphinic groups provides a hint for the position of the hydrolytic water: ~3Å from the zinc ion and H-bonded to the carboxyl group of Glu-296. The distance observed for this H bond (2.4–2.5Å) implies a low-barrier H bond, which is appropriate for the proton transfer associated with Glu-296 during the nucleophilic attack by water.

There is controversy regarding the position of the hydrolytic water in catalytic zinc sites. In the literature, proposals for catalytic mechanisms involving both direct zinc-water coordination, as well as more distant zinc-water interaction, exist (see Lipscomb and Strater [1996] for a review). Our structures indicate that the coordination chemistry around the zinc ion, in the substrate bound form, appears to prevent formation of an excessively short, strong zinc-water coordinate bond, which could lead to entrapment of a Zn-OH species. Consequently, for M1 APs, our data support a position of the hydrolytic water compatible with weak zinc coordination and relatively strong H bonding to Glu-296. Such a positioning would still allow the acidity of the hydrolytic water to increase, thereby facilitating the action of Glu-296, without risking formation of a Zn-OH kinetic trap.

Glu-296 Shuffles Protons to the Leaving Amine

To create a good leaving group, allowing the peptide to break apart, the leaving amine must acquire an additional proton. Based on mutagenesis, Tyr-383 was previously proposed to act as an acid catalyst for this purpose (Blomster et al., 1995). However, we find that Tyr-383 is too far from the amine nitrogen, and nothing in the structure suggests that the pKa of Tyr-383 is unusually low—to the contrary, calculations indicate that it is increased. The most obvious acid catalyst is Glu-296, protonated as a consequence of the previous catalytic step. In this way, the newly formed glutamic acid shuffles a proton to the leaving amine (Figures 4C and 4D). This is equivalent to a proposed function for the corresponding Glu in thermolysin (Matthews, 1988).

To model binding of a proper reaction intermediate, we constructed such a species starting from the structure judged to most closely resemble the transition state. Thus, one of the bound inhibitors was rebuilt into a hydrated peptide of the sequence Arg-Ala-Ala and its binding conformations optimized by molecular mechanics and quantum chemical approaches.

Optimization yielded a conformation optimal for Glu-296 to act as a proton shuffle to the leaving amine nitrogen and direct transfer of a proton to its lone-pair (Figures 4C and 4D, Figure S3).

Zinc-Coordinating Groups of the Substrate Are Exchanged During the Reaction, but the Overall Metal Coordination Is Maintained

The α-amino group of the bound RSR interacts with Glu-271, Glu-318, and the zinc ion. The short distance (2.0Å) to the zinc ion implies that the amino group exists in neutral form and creates a direct coordinate bond with that ion. Because the free amine of RB3040 or RB3041 exhibits no corresponding interaction, this bond may form only in the initial enzyme-substrate complex, as previously proposed for aminopepdidase N (Figures 4A and 4B) (Luciani et al., 1998). This exchange of zinc-coordinating groups implies that the position of the substrate is slightly shifted during the reaction (Figures 4B and 4C).

Because the protonated form of the α-amine group dominates over the neutral form in aqueous solution at pH 7, this group must be neutralized to allow the peptide to bind as outlined above. An obvious candidate to catalyze this deprotonation is Glu-271, because a glutamine is not accepted at this position (Iturrioz et al., 2001; Laustsen et al., 2001; Luciani et al., 1998; Rudberg et al., 2002a). In LTA4H•RB3040 and LTA4H•RB3041, proper zinc coordination is obtained through chelation by the phosphinic moiety. Given the positional certainty of the coordinates, the amine-zinc coordinate bond is doubtlessly absent in the inhibitor complexes. As suggested by previous mutational data, the lost zinc-amine coordinate bond is compensated by a strengthened interaction between Glu-271 and the substrate's amine (Figures 4B and 4C). Even though this is observed in the present structures, uncertainty in coordinates makes it impossible to fully confirm this notion. As for the *tri*peptides, the free amine of the inhibitors also forms H bonds with the carboxylic oxygens of Glu-318 and additionally forms a new H bond with Gln-136.

Zinc coordination geometry appears to be critical for ligand binding and is basically maintained throughout the reaction. Thus, bound substrate, inhibitor, or reaction intermediates must provide the fourth zinc binding ligand at a distance close to 2Å and a fifth, slightly more distant ligand (Figures 4A–4D). This type of coordination pattern is observed in certain other catalytic zinc sites (Alberts et al., 1998).

SIGNIFICANCE

LTA4H belongs to the M1 family of APs, which includes enzymes with a broad range of biological activities. M1 APs share significant overall sequence similarity, including the conserved HEXXH-X_{18}-E motif and the GXMEN motif. Our data indicate that the latter motif is the structural consensus motif for the exopeptidase activity of M1 APs. The α-amino group of peptide substrates binds to the glutamate of this motif and is directly coordinated by the catalytic zinc. The substrate backbone also aligns and binds along this motif. Catalysis of peptide bond hydrolysis relies on residues fully conserved within this enzyme family. Therefore, our conclusions about catalysis and the main structural determinants required for overall substrate binding likely hold true for all M1 APs.

EXPERIMENTAL PROCEDURES

Material

All standard chemicals were obtained from Sigma. Restriction enzymes and chemicals for PCR were obtained from Invitrogen. Reagents for determination of protein concentration were obtained from Bio-Rad. Custom-made peptides were obtained from KJ Ross-Petersen.

Synthesis of Transition State Analogs

For good resemblance of the inhibitors with the main transition state for hydrolysis of *tri*peptides (i.e., the preferred substrate of LTA4H), inhibitors were selected to have backbones with such chain lengths. We reasoned that identical substrate and inhibitor chain length is important for accurate mimicry and excludes secondary effect on the overall binding pattern.

Synthesis was performed as previously described and inhibitors denoted RB3040 ((*S*)-2-((*S*)-2-(2-(((*R*)-1-aminoethyl)(hydroxy)phosphoryl)acetamido)-3-(biphenyl-4-yl)propanamido)propanoic acid) and RB3041 ((*S*)-2-((*S*)-2-(2-(((*R*)-1-amino-2-phenylethyl)(hydroxy)phosphoryl)acetamido)-3-phenylpropanamido)-3-phenylpropanoic acid) (Chen et al., 2000).

Mutagenesis, Protein Expression, and Purification

Site-directed mutagenesis was performed with the QuickChange method (Stratagene). Mutations were verified by DNA sequencing by KI Seq (Karolinska Institute). His-tagged recombinant protein was expressed in *E. coli* JM101 and purified as described (Rudberg et al., 2002a). The yield was ~2.2 mg/l cell culture. Purified protein appeared as a single band on a Coomassie-stained SDS-PAGE gel. Protein concentration was determined by the Bradford method.

Crystallization

RB3040 or RB3041 was co-crystallized with LTA4H by liquid-liquid diffusion in melting-point capillaries. A Tris solution (10 mM [pH 7.5]) of protein and inhibitor (equimolar concentrations, ~70 μM) was layered on the precipitate solution (28% [weight/volume] polyethylene glycol [M_w 8000], 50 mM Na acetate, 100 mM imidazole [pH 6.8], and 5 mM $YbCl_3$). For cocrystallization of *tri*peptides and [E296Q]LTA4H, conditions were identical, except that ligand concentration was increased 10-fold.

Data Collection and Processing

Data were collected at beamlines I-711 and I-911 (MAX lab II, Lund, Sweden). Peptide-containing crystals were additionally soaked in 14% (weight/volume) polyethylene glycol (M_w 8000), 25 mM sodium acetate, 50 mM imidazole (pH 6.8), 2.5 mM $YbCl_3$, and 1 mM *tri*peptide for 12 h. For data collection under cryogenenic conditions, crystals were frozen in the same solutions used for soaking or crystallization, supplemented with 25% (vol/vol) glycerol. Complete data sets were obtained from single crystals. Data sets were processed with XDS or Mosflm followed by Scala and other programs of the CCP4 suite (CCP 4, 1994; Kabsch, 1993; Leslie, 1992).

Model Refinement

Crystals were isomorphous with previously analyzed [E271Q]LTA4H crystals (PDB accession id: 1H19). This structure, stripped of all ligands and water molecules, was used for initial rigid body refinement. For all data sets, 3.3% of the data was set aside for cross-validation.

For [E296Q]LTA4H•RAR, LTA4H•RB3040, and LTA4H•RB3041 crystals, CNS was used for initial refinement (Brünger et al., 1987). After several rounds of refinement and manual model building with Xtalview (McRee, 1999), Refmac5 was used (Murshudov et al., 1997). Topology files for RB3040 and RB3041 were generated with the sketcher facility of the CCP4 suite.

For the [E296Q]LTA4H•RSR crystal, structure refinement was performed with Shelxl (Sheldrick and Schneider, 1997). Some residues were modeled with alternative side chain conformations, B-factors refined using anisotropy, and riding hydrogens added to the model, all while monitoring the Rfree value. The final refinement included the cross-validation data.

Molecular Modeling

To obtain a view of the binding conformation of a proper reaction intermediate, such a species was constructed from RB3040 bound to the active site of

LTA4H. The rationale was that the binding conformation of RB3040 is likely to be very close to that of a real tetrahedral reaction intermediate and that this conformation could be reached by energy minimization. Thus, the structure of RB3040 bound to the active site of LTA4H was minimally rebuilt to that of an Arg-Ala-Ala hydrated *tri*peptide. Glu-296 was protonated, since the hydrated peptide represents the specific reaction intermediate formed as a consequence of the action of this residue as a base catalyst. The geometry of the hydrated *tri*peptide was optimized with MOPAC using the AM1 Hamiltonian (Stewart, 1990). The binding conformation was optimized with the AMBER99 force field (Wang et al., 2000) via steepest-descent minimization and simulated annealing until convergence was reached. As implied by the [E296Q]LTA4H•RSR crystal structure, the α-amine of the bound peptide species was modeled in neutral form.

An orthorhombic simulation cell (extending 7.5 Å in each direction of the protein), explicit water molecules, an all atom model and periodic boundary conditions were used. Residue pKa values were assigned, and the cell content neutralized with sodium ions (Krieger et al., 2006). Long-range electrostatics were treated by the Particle Mesh Ewald algorithm (Essmann et al., 1995). A 15 Å cutoff was used for other nonbonding interactions. To avoid problems with the zinc coordination sphere, the zinc ion and its coordinating atoms were fixed during simulations. The above modeling steps were performed with YASARA (Krieger et al., 2004).

Because molecular mechanics methods do not describe zinc coordination properly and model unstable reaction intermediates poorly, we used the hybrid quantum chemical/molecular mechanics (QM/MM) approach of the QSite 4.0 software (Schrödinger, LLC, New York, NY) to verify the binding mode of the reaction intermediate by further geometry optimization. In this QM/MM energy minimization process, the ligand, the zinc ion, and its coordinating residues were described at the quantum mechanical level (DFT-B3LYP/lacvp**). The rest of the protein was described by molecular mechanics with the OPLS_2001 force field.

Enzyme Activity Determination by Initial Velocity Experiments

Peptidase activity assays were performed in 96-well plates with Ala-*p*-NA or Arg-*p*-NA as substrates as described (Tholander et al., 2005). For wild-type enzyme, each reaction mixture contained 1 μg of protein, as described, whereas for mutants with low activity, the amount of protein was increased 10 to 100 times to obtain detectable signals. To determine kinetic parameters, the Michaelis-Menten rate-law equation were fitted to the data by appropriate least-squares regression methods.

Determination of Inhibition Kinetics via Progress-Curve Analysis

The inhibition potencies and the slow-binding properties of the inhibitors RB3040 and RB3041 were obtained via progress-curve analysis (Duggleby, 2001; Duggleby and Szedlacsek, 1995; Plesner et al., 2001). Aliquots (50 μl) containing 0.29 μM enzyme and 500 mM KCl in 250 mM Tris buffer (pH 7.5) were added to reaction wells of a multiwell plate. Reactions were initiated by addition of 200 μl 1750 μM Ala-*p*-NA with increasing amounts of inhibitor (0.0625-5 μM). After brief mixing, *p*-NAn (*para*-nitroaniline) formation was monitored by measuring absorbance at 405 nm every 10 s for ~60 min. Kinetic parameters were determined by analyzing progress curve data with Dynafit, a dedicated software that numerically solves and fits the set of differential equations, which are defined by the kinetic system under study, to the experimental data (Kuzmic, 1996). The mechanistic model that best described the data was: $S + E \rightarrow SE \rightarrow P + E$, $E + I \leftrightarrow EI$. During fitting of kinetic models, concentrations were treated as local parameters with 50% certainty, and all kinetic parameters were allowed to vary.

ACCESSION NUMBERS

Atomic coordinates and structure factors are available in the Protein Data Bank (http://www.rcsb.org/) at: 3B7R (LTA4H•RB3040), 2R59 (LTA4H•RB3041), 3B7S ([E296Q]LTA4H•Arg-Ser-Arg), and 3B7T ([E296Q]LTA4H•Arg-Ala-Arg).

SUPPLEMENTAL DATA

Supplemental Data include four figures, one table, and Supplemental References and can be found with this article online at http://www.chembiol.org/cgi/content/full/15/9/920/DC1/.

ACKNOWLEDGMENTS

The authors thank Eva Ohlson for technical assistance and the personnel at the I711 and I911 beam-lines of the MAX-Lab synchrotron facility for assistance with data collection. The work was funded by The Swedish Research Council (03X-10350), the CIDaT consortium (Vinnova), and EC FP6 (LSHM-CT-2004-005033). This report reflects the views of the author; the European Commission is not liable for any use that may be made of the information herein.

Received: April 17, 2008
Revised: July 26, 2008
Accepted: July 31, 2008
Published: September 19, 2008

REFERENCES

Alberts, I.L., Nadassy, K., and Wodak, S.J. (1998). Analysis of zinc binding sites in protein crystal structures. Protein Sci. *7*, 1700–1716.

Andberg, M., Wetterholm, A., Medina, J.F., and Haeggström, J.Z. (2000). Leukotriene A4 hydrolase: a critical role of glutamic acid-296 for the binding of bestatin. Biochem. J. *345*, 621–625.

Barret, A.J., Rawlings, N.D., and Woessner, J.F. (1998). Catalytic mechanisms for metallopeptidases. In Handbook of Proteolytic Enzymes, Second Edition, A.J. Barret, N.D. Rawlings, and J.F. Woessner, eds. (San Diego: Academic Press), pp. 268–289.

Beaumont, A., O'Donohue, M.J., Paredes, N., Rousselet, N., Assicot, M., Bohuon, C., Fournie-Zaluski, M.C., and Roques, B.P. (1995). The role of histidine 231 in thermolysin-like enzymes. A site-directed mutagenesis study. J. Biol. Chem. *270*, 16803–16808.

Blomster, M., Wetterholm, A., Mueller, M.J., and Haeggström, J.Z. (1995). Evidence for a catalytic role of tyrosine 383 in the peptidase reaction of leukotriene A_4 hydrolase. Eur. J. Biochem. *231*, 528–534.

Breidenbach, M.A., and Brunger, A.T. (2004). Substrate recognition strategy for botulinum neurotoxin serotype A. Nature *432*, 925–929.

Brünger, A.T., Kuriyan, J., and Karplus, M. (1987). Crystallographic R factor refinement by molecular dynamics. Science *235*, 458–460.

Chen, H., Noble, F., Coric, P., Fournie-Zaluski, M.C., and Roques, B.P. (1998). Aminophosphinic inhibitors as transition state analogues of enkephalin-degrading enzymes: a class of central analgesics. Proc. Natl. Acad. Sci. USA *95*, 12028–12033.

Chen, H., Noble, F., Mothe, A., Meudal, H., Coric, P., Danascimento, S., Roques, B.P., George, P., and Fournie-Zaluski, M.C. (2000). Phosphinic derivatives as new dual enkephalin-degrading enzyme inhibitors: synthesis, biological properties, and antinociceptive activities. J. Med. Chem. *43*, 1398–1408.

CCP4 (Collaborative Computing Project, Number 4). (1994). The CCP4 suite: programs for protein crystallography. Acta Crystallogr. D Biol. Crystallogr. *50*, 760–763.

Duggleby, R.G. (2001). Quantitative analysis of the time courses of enzyme-catalyzed reactions. Methods *24*, 168–174.

Duggleby, R.G., and Szedlacsek, S.E. (1995). Kinetics of slow and tight-binding Inhibitors. Methods Enzymol. *249*, 144–180.

Essmann, U., Perera, L., Berkowitz, M.L., Darden, T., Lee, H., and Pedersen, L.G. (1995). A smooth particle mesh Ewald method. J. Chem. Phys. *103*, 8577–8593.

Haeggström, J.Z. (2004). Leukotriene A4 hydrolase/aminopeptidase, the gatekeeper of chemotactic leukotriene B4 biosynthesis. J. Biol. Chem. *279*, 50639–50642.

Iturrioz, X., Rozenfeld, R., Michaud, A., Corvol, P., and Llorens-Cortes, C. (2001). Study of asparagine 353 in aminopeptidase A: characterization of a novel motif (GXMEN) implicated in exopeptidase specificity of monozinc aminopeptidases. Biochemistry *40*, 14440–14448.

Kabsch, W. (1993). Automatic processing of rotation diffraction data from crystals of initially unknown symmetry and cell constants. J. Appl. Cryst. *26*, 795–800.

Krieger, E., Darden, T., Nabuurs, S.B., Finkelstein, A., and Vriend, G. (2004). Making optimal use of empirical energy functions: force-field parameterization in crystal space. Proteins *57*, 678–683.

Krieger, E., Nielsen, J.E., Spronk, C.A., and Vriend, G. (2006). Fast empirical pKa prediction by Ewald summation. J. Mol. Graph. Model. *25*, 481–486.

Kuzmic, P. (1996). Program DYNAFIT for the analysis of enzyme kinetic data: application to HIV proteinase. Anal. Biochem. *237*, 260–273.

Laustsen, P.G., Vang, S., and Kristensen, T. (2001). Mutational analysis of the active site of human insulin-regulated aminopeptidase. Eur. J. Biochem. *268*, 98–104.

Leslie, A.G.W. (1992). Recent changes to the MOSFLM package for processing film and image plate data. In Joint CCP4 and ESF-EACMB Newsletter on Protein Crystallography No. 26 (Warrington, UK: Daresbury Laboratory).

Lipscomb, W.N., and Strater, N. (1996). Recent advances in zinc enzymology. Chem. Rev. *96*, 2375–2434.

Luciani, N., Marie-Claire, C., Ruffet, E., Beaumont, A., Roques, B.P., and Fournie-Zaluski, M.C. (1998). Characterization of Glu350 as a critical residue involved in the N-terminal amine binding site of aminopeptidase N (EC 3.4.11.2): insights into its mechanism of action. Biochemistry *37*, 686–692.

Matthews, B.W. (1988). Structural basis of the action of thermolysin and related zinc peptidases. Acc. Chem. Res. *21*, 333–340.

McRee, D.E. (1999). XtalView/Xfit–A versatile program for manipulating atomic coordinates and electron density. J. Struct. Biol. *125*, 156–165.

Medina, J.F., Wetterholm, A., Rådmark, O., Shapiro, R., Haeggström, J.Z., Vallee, B.L., and Samuelsson, B. (1991). Leukotriene A_4 hydrolase: determination of the three zinc-binding ligands by site-directed mutagenesis and zinc analysis. Proc. Natl. Acad. Sci. USA *88*, 7620–7624.

Minami, M., Bito, H., Ohishi, N., Tsuge, H., Miyano, M., Mori, M., Wada, H., Mutoh, H., Shimada, S., Izumi, T., et al. (1992). Leukotriene A4 hydrolase, a bifunctional enzyme. Distinction of leukotriene A4 hydrolase and aminopeptidase activities by site-directed mutagenesis at Glu-297. FEBS Lett. *309*, 353–357.

Mock, W.L., and Aksamawati, M. (1994). Binding to thermolysin of phenolate-containing inhibitors necessitates a revised mechanism of catalysis. Biochem. J. *302*, 57–68.

Mock, W.L., and Stanford, D.J. (1996). Arazoformyl dipeptide substrates for thermolysin. Confirmation of a reverse protonation catalytic mechanism. Biochemistry *35*, 7369–7377.

Murshudov, G.N., Vagin, A.A., and Dodson, E.J. (1997). Refinement of macromolecular structures by the maximum-likelihood method. Acta Crystallogr. D Biol. Crystallogr. *53*, 240–255.

Örning, L., Gierse, J.K., and Fitzpatrick, F.A. (1994). The bifunctional enzyme leukotriene A4 hydrolase is an arginine aminopeptidase of high effiency and specificity. J. Biol. Chem. *269*, 11269–11273.

Phillips, M.A., Fletterick, R., and Rutter, W.J. (1990). Arginine 127 stabilizes the transition state in carboxypeptidase. J. Biol. Chem. *265*, 20692–20698.

Plesner, I.W., Bulow, A., and Bols, M. (2001). Accurate determination of rate constants of very slow, tight-binding competitive inhibitors by numerical solution of differential equations, independently of precise knowledge of the enzyme concentration. Anal. Biochem. *295*, 186–193.

Rawlings, N.D., Tolle, D.P., and Barrett, A.J. (2004). MEROPS: the peptidase database. Nucleic Acids Res. *32*, D160–D164.

Robertus, J.D., Kraut, J., Alden, R.A., and Birktoft, J.J. (1972). Subtilisin; a stereochemical mechanism involving transition-state stabilization. Biochemistry *11*, 4293–4303.

Rudberg, P.C., Tholander, F., Thunnisen, M.G.M., and Haeggström, J.Z. (2002a). Leukotriene A_4 hydrolase/aminopeptidase: glutamate 271 is a catalytic residue with specific roles in two distinct enzyme mechanisms. J. Biol. Chem. *277*, 1398–1404.

Rudberg, P.C., Tholander, F., Thunnissen, M.G.M., Samuelsson, B., and Haeggström, J.Z. (2002b). Leukotriene A4 hydrolase: selective abrogation of leukotriene B4 formation by mutation of aspartic acid 375. Proc. Natl. Acad. Sci. USA *99*, 4215–4220.

Samuelsson, B. (1983). Leukotrienes: mediators of immediate hypersensitivity reactions and inflammation. Science *220*, 568–575.

Schechter, I., and Berger, A. (1967). On the size of the active site in proteases. I. Papain. Biochem. Biophys. Res. Commun. *27*, 157–162.

Sheldrick, G.M., and Schneider, T.R. (1997). SHELXL: high-resolution refinement. Methods Enzymol. *277*, 319–343.

Stewart, J.J.P. (1990). MOPAC: a semi-empirical molecular-orbital program. J. Comput. Aided Mol. Des. *4*, 1–45.

Tholander, F., and Haeggström, J.Z. (2007). Assay for rapid analysis of the tri-peptidase activity of LTA4 hydrolase. Proteins *67*, 1113–1118.

Tholander, F., Kull, F., Ohlson, E., Shafqat, J., Thunnissen, M.M., and Haeggstrom, J.Z. (2005). Leukotriene A4 hydrolase, insights into the molecular evolution by homology modeling and mutational analysis of enzyme from Saccharomyces cerevisiae. J. Biol. Chem. *280*, 33477–33486.

Thunnissen, M.M.G.M., Nordlund, P., and Haeggström, J.Z. (2001). Crystal structure of human leukotriene A(4) hydrolase, a bifunctional enzyme in inflammation. Nat. Struct. Biol. *8*, 131–135.

Turk, B.E., Wong, T.Y., Schwarzenbacher, R., Jarrell, E.T., Leppla, S.H., Collier, R.J., Liddington, R.C., and Cantley, L.C. (2004). The structural basis for substrate and inhibitor selectivity of the anthrax lethal factor. Nat. Struct. Mol. Biol. *11*, 60–66.

Wang, J., Cieplak, P., and Kollman, P.A. (2000). How well does a restrained electrostatic potential (RESP) model perform in calculating conformational energies of organic and biological molecules? J. Comput. Chem. *21*, 1049–1074.

Wetterholm, A., Medina, J.F., Rådmark, O., Shapiro, R., Haeggström, J.Z., Vallee, B.L., and Samuelsson, B. (1992). Leukotriene A_4 hydrolase: abrogation of the peptidase activity by mutation of glutamic acid-296. Proc. Natl. Acad. Sci. USA *89*, 9141–9145.